

Luminescent Solar Concentrators for Greenhouse Applications Based on Highly Luminescent Carbon Quantum Dots

Kambiz Hosseinpanahi, Mohammad Hossein Abbaspour-Fard,*
Mahmoud Reza Golzarian, Elaheh K. Goharshadi, and Alberto Vomiero*

Carbon quantum dots (CQDs) are promising luminophores for luminescent solar concentrators (LSCs) in transparent photovoltaic greenhouse covers due to their high ultraviolet (UV)-light absorption coefficient, which is vital for plant growth. Herein, high quantum yield (75%) and large Stokes shift (0.706 eV) CQDs are synthesized by a simple, fast, cheap, and mass scalable method. A comprehensive study on the LSC engineering is carried out. Thin layers of CQDs with different concentrations of 1, 3, and 5 wt% and different number of layers (1–5) are coated on glass and poly(methyl methacrylate) (PMMA) waveguides, sized $5 \times 5 \times 0.6$ and $15 \times 15 \times 0.6$ cm³. The best performing single-layer LCS exhibits power conversion efficiency (PCE) and optical efficiency as high as 1.6% and 6.5%, respectively (LSC size $5 \times 5 \times 0.6$ cm³), and 1.19% and 3.27% (LSC size of $15 \times 15 \times 0.6$ cm³), respectively. Over 90 days, stability tests show a 2% PCE decrease. Tests on a small-scale greenhouse model demonstrate that transparent photovoltaic LSC roofs not only produce electricity but also control temperature inside the greenhouse. Hence, CQD-based LSCs synthesized by the scalable method can be used in commercialization of transparent greenhouses photovoltaic covers.


1. Introduction

One of the new ways to produce sufficient and quality food is the expansion of new cultivation strategies, such as vertical farming, and their combination with methods such as hydroponic and aeroponic cultivation greenhouses. The use of new cultivation systems increases the yield of crops up to 11 times, but at the same time, it can also increase the amount of energy consumption up to more than 80 times.^[1] This massive increase in energy consumption is due to the need for more input energy to provide light, irrigation, temperature regulation, transmission of strengthening treatments, and use of other equipment to provide suitable environmental conditions for plant growth.^[1,2] Fossil fuels must be used directly or indirectly to supply this energy in modern agriculture systems. The extensive use of fossil fuels in modern greenhouse, in addition to creating

K. Hosseinpanahi, M. H. Abbaspour-Fard
Department of Biosystems Engineering
Faculty of Agriculture
Ferdowsi University of Mashhad
Mashhad 9177948974, Iran
E-mail: abaspour@um.ac.ir

M. R. Golzarian
School of Information Technology
Murdoch University
WA 6150, Australia

M. R. Golzarian
School of Science
Edith Cowan University
WA 6027, Australia

 The ORCID identification number(s) for the author(s) of this article can be found under <https://doi.org/10.1002/solr.202400442>.

© 2024 The Author(s). Solar RRL published by Wiley-VCH GmbH. This is an open access article under the terms of the Creative Commons Attribution License, which permits use, distribution and reproduction in any medium, provided the original work is properly cited.

DOI: 10.1002/solr.202400442

E. K. Goharshadi
Department of Chemistry
Faculty of Science
Ferdowsi University of Mashhad
Mashhad 9177948974, Iran

E. K. Goharshadi
Nano Research Center
Ferdowsi University of Mashhad
Mashhad 9177948974, Iran

A. Vomiero
Division of Materials Science
Department of Engineering Sciences and Mathematics
Luleå University of Technology
97187 Luleå, Sweden
E-mail: alberto.vomiero@ltu.se

A. Vomiero
Department of Molecular Sciences and Nanosystems
Ca' Foscari University of Venice
Via Torino 155, 30172 Venezia Mestre, Italy

A. Vomiero
Istituto di Struttura della Materia (ISM) - CNR
S.S. 14 Km 163.5, I-34149 Trieste, Italy

environmental problems and unsafe food production, due to the price fluctuations of these fuels, will negatively impact the price and the product quality. One of the energy supply solutions in greenhouses based on modern cultivation systems is to turn to the concept of agrivoltaic in greenhouse. Due to the need for the most intelligent systems for electricity, the photovoltaic greenhouse can provide a large part of its energy demand. In this regard, many researches performed on the development of photovoltaic greenhouses have generally been in the form of installing silicon solar panels in different arrangements on the roof of the greenhouse.^[2–6] The results of the investigations show that the shadow created by installing silicon solar panels on the greenhouse roof affects the plant growth negatively. In general, the increase of shadows in the greenhouse is the most critical challenge when using (non-transparent) silicon photovoltaic panels.^[2–4,7–10] Researchers have developed transparent/semi-transparent greenhouse covers to address this challenge using transparent solar cells technologies. These greenhouse photovoltaic transparent covers produce electricity as light passes through them.^[10–17] The main challenge is to balance two conflicting properties, that is, light transmission and electricity generation. In fact, light must be absorbed to produce electricity, while the greenhouse cover must have proper transparency and light transmission to allow the photosynthetic activity of greenhouse plants to occur. Therefore, the most critical challenge is the development of a photovoltaic cover, which is transparent in the spectral range useful for the plant, and which can absorb other wavelengths that are unnecessary or harmful for the plant, like, for instance, the ultraviolet (UV) light, which can generate electrical power. In other words, the photovoltaic cover of the greenhouse should balance food production from the point of view of light management and the physiological needs of the plant, and energy production. Among various photovoltaic technologies, luminescent solar concentrators (LSCs) can be used in making transparent photovoltaic greenhouse covers. They are made of a glass or polymer matrix covered or doped with a luminescent material which absorbs light in a specific spectral range and emits light in another spectral range with a longer wavelength inside the waveguide. The light emitted through the lateral edges reaches the thin strips of the solar cell and electric power is produced (**Figure 1a**). The distinctive features of LSCs have caused them to be used in greenhouse photovoltaic covers. Also, LSCs improve the production efficiency of agricultural products by converting UV light to useful light spectrums in the visible range.^[12–14,18]

The essential advantages of LSCs for use as photovoltaic greenhouse covers are:^[12,19–21] 1) They absorb all direct and scattered lights due to the presence of luminophores, and unlike other solar technologies, there is no need for solar tracking equipment, which is an outstanding feature for photovoltaic greenhouse covers, usable on both the roof and even the greenhouse walls; 2) The amount of light absorption by the cells located at the edges is very high because the surface exposed to the light is much larger than the area of the edges; 3) There is a possibility to convert harmful light spectrum into useful light spectrum for the plant; 4) It has simple and cheap fabrication; 5) The color, transparency, and light absorption can be controlled with changes in the properties of luminophores; 6) It can be used in different environments in terms of aesthetics.

In general, the most crucial advantage of LSC technology as a photovoltaic greenhouse cover for developing an agrivoltaic system is to balance food and energy production. An excellent luminescent material for use in LSCs for greenhouse cover must have a high light absorption coefficient in the range of wavelengths that are unnecessary or not useful for the plant, have a high photoluminescence (PL) quantum yield, have no overlap between the absorption and the emission spectrum (large Stokes shift) to minimize the reabsorption losses, and have good chemical and optical stability when placed inside the waveguide.^[19,20,22] Among different luminescent materials, carbon quantum dots (CQDs) have attracted a huge interest, due to their non-toxic and abundant elemental composition such as carbon, nitrogen, and oxygen, simple, low-cost, and environmentally friendly synthesis on a large scale, adjustable absorption-emission spectrum, high quantum yield, and excellent thermal and optical stability.^[19,23–26] One of the optical capabilities of CQDs is the absorption of light in the UV region. On the contrary, UV light has destructive and irreparable effects on plant growth by 1) Weakening of photosynthesis, 2) Indirect effect on secondary metabolism causing a significant increase in insects, fungi, and other pathogenic agents, 3) Making biochemical changes on insects and as a result, insects tend to consume plant tissue, 4) Causing plant gravity against pests through DNA damage, changes in secondary metabolisms and changes in leaf analogues, leaf thickness, and cuticle thickness.^[27–29] This feature further demonstrates the capability of CQDs in the construction of LSCs for use as transparent/semi-transparent photovoltaic greenhouse covers. The LSC based on CQDs, prevents the UV light from entering the greenhouse. Instead of reflecting it, it absorbs the UV light and converts it into longer wavelengths that are useful for both the plant, if they fall within the escape cone of the LSC, and electric power generation. Considering the good capabilities of CQDs in the development of transparent photovoltaic greenhouse covers based on LSCs, to scale up and finally commercialize, cheap and scalable synthesis methods for CQDs with high quantum yield and high Stokes shift should be developed practically.^[19,30,31] Herein, we developed a new generation of transparent photovoltaic greenhouse cover using LSCs based on CQDs with a high quantum yield, synthesized by a scalable, cheap, and fast method.^[31] One of the common challenges in the synthesis of QDs is their PL quenching due to aggregation-induced quenching (AIQ) after their synthesis. To address this challenge, CQDs are prepared in the form of sponge or foam.^[30–33] It leads to the scalable and high quantum yield synthesis of CQDs with a high Stokes shift.^[31] Furthermore, we investigated experimentally some of the most critical parameters affecting the efficiency of LSC including the type of waveguide, the concentration of the luminophores, and the number of luminescent layers on the waveguide, so that the LSC fabrication process is engineered and can be repeated under the same laboratory conditions for benchmarking purposes. Then the optical and photovoltaic properties of large-area LSCs ($15 \times 15 \times 0.6 \text{ cm}^3$) were investigated. Finally, a small-scale greenhouse environment with a roof made of an optimized LSC was constructed, and its thermal parameters were investigated in the presence of a transparent photovoltaic cover under sun irradiation.

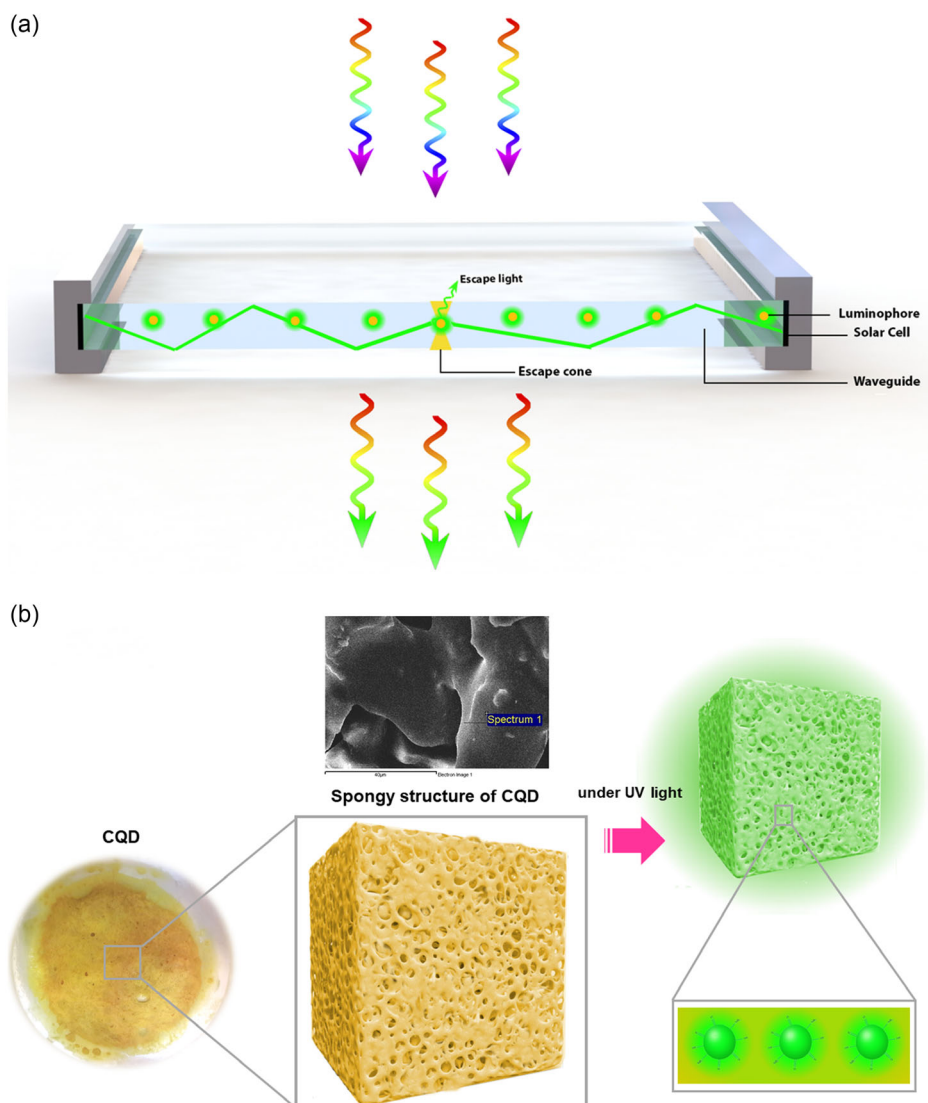


Figure 1. a) Schematic of LSC. As a result of the sunlight incident on the waveguide, a part of the light (here the UV light) is absorbed by the CQDs and its emission (here the green emission) reaches the edges of the waveguide. Part of the light also leaves the surface of the LSC due to losses caused by the escape cone and resorption. b) Schematic of the spongy and porous structure of CQDs formed in presence of NaOH. The SEM image of the spongy structure also confirms this scheme.

2. Materials and Methods

2.1. Synthesis of CQDs

Citric acid (0.0052 mol), urea (0.0333 mol), and NaOH (0.02 mol) were mixed with 20 mL deionized water under 10 min sonication. The solution was placed in the microwave at 1000 W for 3 min. The prepared spongy CQD was washed with ethanol and centrifuged.^[31] To prepare dry CQDs, they were put in a vacuum oven at 60 °C for 24 h. For mass production, the number of precursors was increased by 10 times and the solution was put in the microwave for 25 min (Figure S1 and S2, Supporting Information).

2.2. Fabrication of LSCs

To fabricate the LSCs, first, 10 mL ethanol, 1 g of polyvinylpyrrolidone (PVP) K30, and 1 g of PVP K90 were mixed. The mixture was sonicated for 10 min to obtain a clear solution. Then 1, 3, and 5 wt% of CQDs powder were dissolved in the solution and sonicated for 10 min. Then, it was coated on the surface of the glass and poly(methyl methacrylate) (PMMA) substrate as a waveguide with different dimensions ($5 \times 5 \times 0.6$ and $15 \times 15 \times 0.6 \text{ cm}^3$) by Doctor Blade technique. They were dried for 2 h in an isolated and dark environment. Then the same procedure was used to coat the subsequent layers (1–5 layers). The thickness of the layers in LSCs for 1–5 layers was 5, 12, 18, 23, and 27 μm ,

respectively. The thickness of the layers was measured using a digital micrometer.

2.3. Characterization

The morphology of CQDs was obtained through transmission electron microscopy (TEM) using a Philips EM 208S TEM, through high-resolution TEM (HRTEM) using the Field Electron and Ion company (FEI) model TEC9G20 at 200 kV, and scanning electron microscope (SEM) by LEO-VP 1450. The X-ray diffraction (XRD) pattern of CQDs was recorded using Explorer model of GNR CO. The X-ray photoelectron spectrum (XPS) was obtained using a BESTEC spectrometer (EA 10) equipped with an Al $K\alpha$ X-ray source (15 kV, 50 W). The Fourier transform infrared spectrum (FTIR) spectrum was obtained by a Thermo Nicolet model AVATAR 370 FT-IR spectrometer. A PerkinElmer ls45 device was used to prepare the PL spectrum of CQDs. The absorption and transmission UV-Vis spectra were taken using a Hitachi UH-4150. The PL spectra of the LSCs were obtained using a reflection spectrometer equipped with an optical fiber connected to a solar simulator with an optical spectral range of 200–900 nm. The details were included in the Supporting Information.

3. Results and Discussion

3.1. Synthesis and Characterization of CQDs

CQDs were synthesized based on a scalable, cheap, and fast method using microwaves.^[31] In this method, citric acid and urea were used as precursors, water as a solvent, and NaOH as a crystalline and foamy structure that prevents AIQ during the

formation of CQDs (Figure 1b). CQDs are formed through the processes of dehydration and carbonization between citric acid and urea that occur in the crystal structure of NaOH. This procedure prevents the loss caused by the stacking of carbon dots due to the strong pi–pi stacking between the basal planes of CQDs.^[19,30,31,34,35]

Figure 2a,b show TEM and HRTEM images of prepared CQDs. The HRTEM images of CQDs in Figure 2b shows the lattice fringes with interplanar distance of 0.23 nm of (100) plane of graphene.^[19,30,31] The average particle size of CQDs was calculated and shown in Figure 2c: (3.21 ± 0.78) nm.

The XRD pattern of CQDs in Figure 2d shows the broad peak at about 24.6° corresponds to the reflection of the (002) lattice planes of the graphitic carbon.^[30,31] The reflections at 17.5° , 31° , 1.37° , 41.5° , and 50.7° correspond to the (200), (400), (111), (311), and (020) lattice planes of the crystal structure of monoclinic NaOH.^[31]

The prepared CQDs have high solubility in water probably due to the presence of hydrophilic functional groups such as carboxyl, amide, and hydroxyl on their surface.^[21,30,36] To prove this claim, the FTIR spectrum of CQDs was recorded and shown in Figure 2e. The band at 3466.6 cm^{-1} is related to OH stretching vibrations confirming the presence of hydroxyl group on the surface of CQDs.^[31] The band at 1672.2 cm^{-1} is attributed to the C=O and C=N stretching, respectively. Also, the band at 1599.96 and 1398.64 cm^{-1} are related to C=C and C–N bonds.^[19,30,37]

XPS analysis was performed to investigate the elemental composition of CQDs (Figure 3). As can be seen from Figure 3a, five substantial peaks are found in the structure of CQDs, which are related to carbon (C_{1s}), nitrogen (N_{1s}), oxygen (O_{1s}), and sodium (Na_{1s}). These peaks constitute 52.7%, 15.7%, 26.4%, and 5.2%

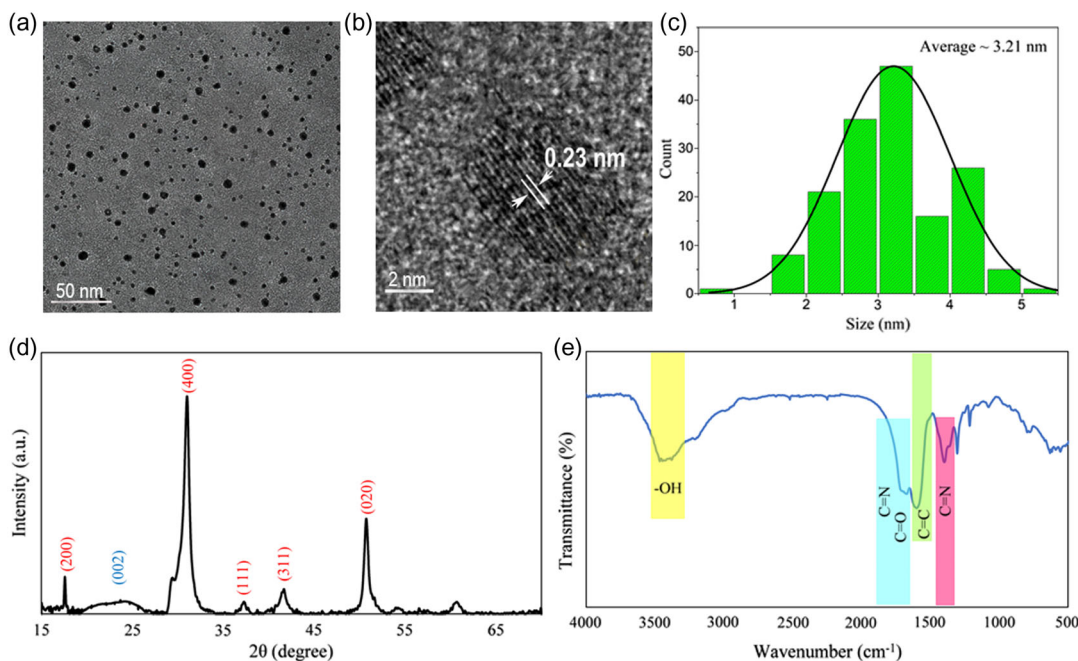


Figure 2. a) TEM, b) HRTEM image of CQDs, c) particle size distribution histogram of synthesized CQDs, d) XRD spectrum, and e) FTIR spectrum of synthesized CQDs.

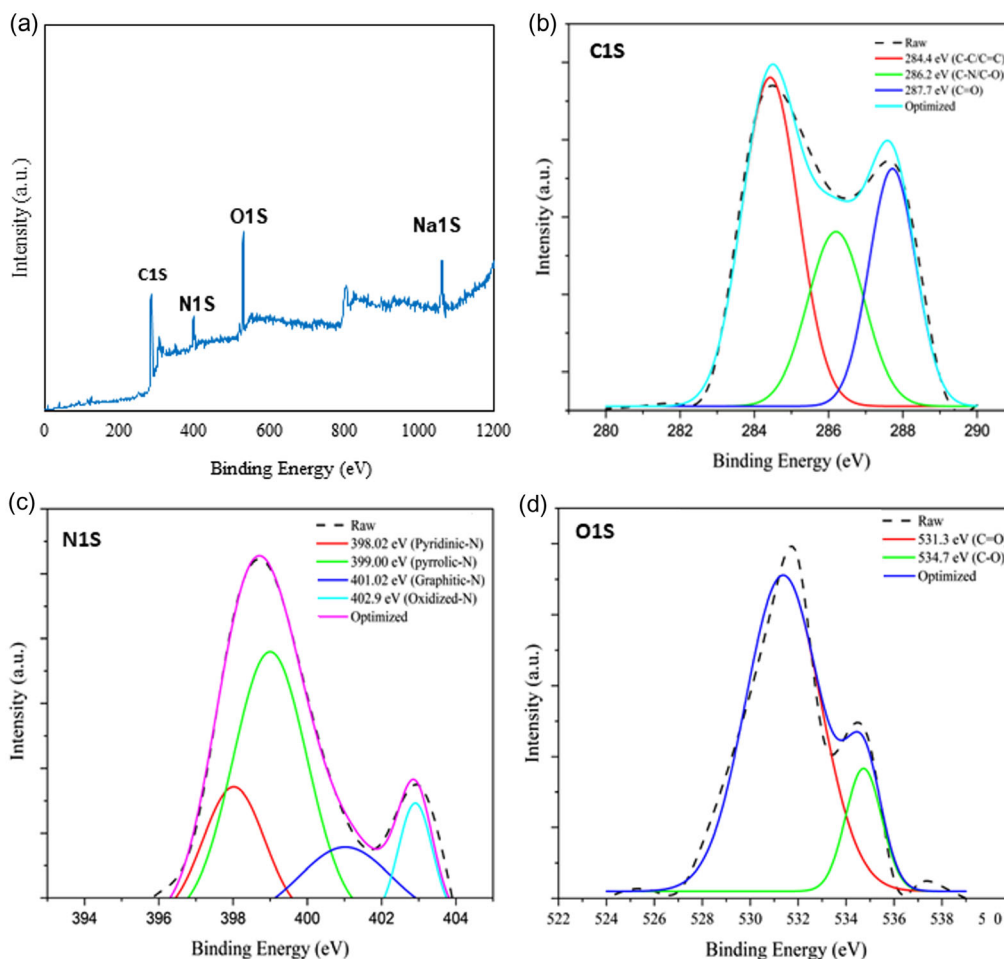


Figure 3. a) XPS survey spectrum of CQDs. b) Deconvolution of XPS spectrum of C_{1S}, c) N_{1S}, and d) O_{1S}.

percent of the structure, respectively. The deconvolution of the high-resolution C_{1S} spectrum showed species at 284.4, 286.2, and 287.7 eV, which are attributed to C–C or C=C, C–N or C–O, and C=O, respectively (Figure 3b). The high-resolution XPS spectrum of N_{1S} can be fitted through four peaks in the regions of 398.02, 399, 401.02, and 402.9 eV, which are assigned to pyridinic, pyrrolic, graphitic, and oxidized nitrogen, respectively. (Figure 3c). The high-resolution XPS spectrum of O_{1S} was decomposed into two peaks corresponding to C=O and C–O at 531.3 and 534.7 eV, respectively (Figure 3d). The higher value of C=O in the O_{1S} spectrum can be influenced by its relatively high value in the C_{1S} spectrum. Also, the presence of Na_{1S} at 1063.33 eV in Figure 3a indicates the presence of sodium in the structure.^[19,22,30,31,38] The amount of sodium in the structure was 5.2%.

The presence of functional groups on the surface and the investigation of the elemental composition, chemical state, and general electronic structure of CQDs, revealed through FTIR and XPS analyses, respectively, suggest that the synthesized CQDs can be utilized as fluorophore material. These CQDs can absorb light within a specific wavelength range and subsequently emit it at longer wavelengths. Additionally, due

to the presence of hydrophilic functional groups, the CQDs exhibit excellent solubility in water. Furthermore, when incorporated into polymer substrates to fabricate LSCs, the CQDs demonstrate remarkable stability in terms of their light absorption and emission properties within the LSC structure.

3.2. Optical Properties of CQDs

The optical properties of CQDs were measured. The absorption spectrum (Figure 4a) shows that CQDs have absorption in the range of 250–500 nm. Two peaks at 330 and 400 nm are related to the $\pi \rightarrow \pi^*$ of sp^2 aromatic carbon, and the $n \rightarrow \pi^*$ transition, due to the presence of C=O and C=N bonds, respectively.^[31,39–42] The absorption range of CQDs includes the absorption of the UV region and a part of the visible range, which shows that they can be used in photovoltaic greenhouse covers as UV filters. The PL spectrum of CQDs shows the emission in the visible region from 410 to 600 nm with the emission peak at 518 nm under the excitation wavelength of 400 nm. According to Figure 4b, CQDs have excitation-independent emission indicating that they have a stable emission center. The complete absorption of UV light (as a harmful spectrum for the plant) and its conversion to visible light

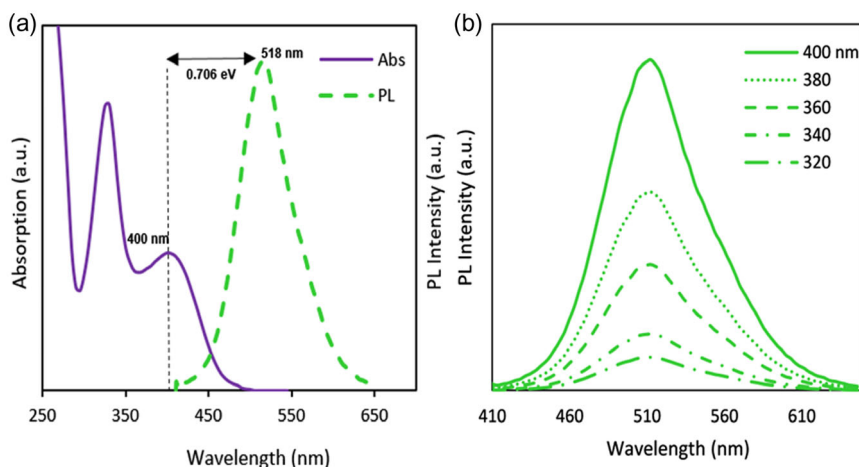


Figure 4. a) Absorption (solid blue line) and emission (green dashed line) spectra of CQDs dispersed in water. b) Emission spectrum of CQDs at different wavelengths from 320 to 400 nm.

(as a beneficial spectrum for the plant) through emission, shows the ability of CQDs as one of the potential structures in the development of photovoltaic greenhouse covers.

The quantum yield of CQDs is 75% (Table S1 and Figure S3, Supporting Information, See the experimental section in the Supporting Information). The high quantum yield of CQDs is attributed to the low non-radiative recombination rate. Also, the Stokes shift of the CQDs is about 0.706 eV (Figure 4a). A higher Stokes shift means a lower reabsorption loss rate. The large Stokes shift and high quantum yield are attributed to the excellent surface passivation of CQDs and appropriate radiative recombination, which is due to the excitation of surface states caused by the $n \rightarrow \pi^*$ transition of surface functional groups. In other words, the large Stokes shift can be attributed to the emission originating from surface states introduced by the carbonyl and nitrogen-containing functional groups, which possess lower energy levels compared to the excitation pathways involving the core and edge states of the CQDs. This separation between absorption and emission energies is a desirable characteristic as it reduces reabsorption, thereby contributing to the high quantum yield of the CQDs. The large Stokes shift significantly reduces reabsorption losses, allowing more of the emitted light to contribute to the LSC instead of being trapped in a repeated cycle of absorption and emission, which would otherwise lead to losses. These conditions improve the radiative transfer rate, resulting in high quantum yield and large Stokes shift.^[30,31,43–45]

3.3. Optical and Photovoltaic Investigation of LSCs

In this part, key parameters such as the waveguide type, luminescent material concentration, and the number of luminescent material layers, which impact the effectiveness and attributes of the greenhouse covering intended for agricultural applications, were studied in the context of LSC fabrication engineering. In determining the type of waveguide, in addition to the optical characteristics, the harshness of the greenhouse environment should also be taken into account, which can influence the

selection of the type of materials. Therefore, to choose the type of waveguide from the photovoltaic point of view, sufficient thickness, suitable optical refractive index, long life, and stability, and from the agricultural point of view, transparency by providing the photosynthetically active radiation spectrum for the plant, suitable life time, and stability of the cover for use as a greenhouse photovoltaic cover are the main parameters which should be considered. Conventional covers are made of polyethylene, polycarbonate, fiberglass, glass, and PMMA. Considering the characteristics of a suitable waveguide to be used as LSC for greenhouse applications mentioned earlier, glass and PMMA are used as waveguides. Glass and PMMA are good options for considering as LSC waveguides due to their high transparency, suitable thickness for solar cell installation at the edges, and good strength and longevity compared to other conventional covers.

For fabrication of LSCs, CQDs with different concentrations of 1, 3, and 5 wt% were mixed with PVP polymer in ethanol and different number of layers, from 1 to 5, were coated on the waveguides (see the experimental section for details on the fabrication of the multilayer structure). The purpose of this work was to maximize the LSC efficiency by optimizing CQD concentration and number of layers. The dimensions of the primary LSCs were $5 \times 5 \times 0.6 \text{ cm}^3$. To investigate the optical and photovoltaic characteristics of large-area LSCs, LSC with dimensions equal to $15 \times 15 \times 0.6 \text{ cm}^3$ was fabricated and tested. The fabricated LSCs with dimensions of $5 \times 5 \times 0.6 \text{ cm}^3$ is shown in **Figure 5** under natural and UV light. The fabricated LSCs have high transparency at a first glance (Figure 5a). Green light emission with high intensity can also be clearly seen from the surface and edge of LSCs under UV light (Figure 5b).

As mentioned, three mass percent of CQDs were used for fabricating LSC. The absorption and emission spectra of LSCs show that by increasing the concentration from 1 to 3 wt%, the intensity of absorption and emission increases. On the contrary, by increasing the concentration of CQDs from 3 to 5 wt%, the intensity of absorption and emission decreases. This process is the same for pure CQDs and in the PVP mixture (Figure S6a–c,

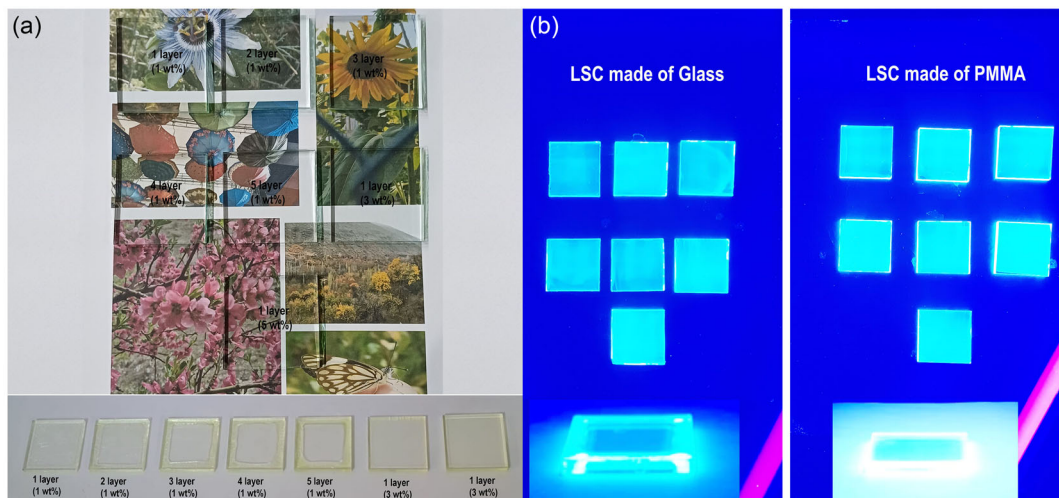


Figure 5. a) Image of LSCs made in different concentrations and number of layers of CQDs on colored test paper and white background to show their apparent transparency. b) Image of LSCs made under UV light. Green emission of quantum dots from the surface and edge of waveguides can be clearly seen.

S7a,c, Supporting Information). The comparison of the absorption and emission spectra of LSCs made with 1–5 layers with a CQD concentration of 1% shows that by increasing the layers from 1 to 4 layers, the intensity of absorption and emission increases. For 5 layers the intensity of absorption and emission spectra decrease (Figure S6d,e and S7b,d, Supporting Information). This reduction in absorption and emission intensity for 5 layers and 5 wt% is attributed to AIQ or worsening of optical properties due to the aggregation of CQDs.^[19,30,31,46,47] To investigate the effect of concentration in one layer more closely, an LSC with a concentration of 4 wt% was also made. The overall results show that the intensity of absorption and emission in the LSC fabricated with a concentration of 3 wt% of the monolayer is much higher than the other LSCs (Figure S6, Supporting Information). To find the reason, the optical refractive index of both waveguides was calculated using the Equation (S5), Supporting Information. The refractive index of glass and PMMA is equal to 1.32 and 1.46, respectively. A host matrix with refractive index in the range $1.5 < n < 2$ is widely preferred to reduce escape-cone losses.^[48] By examining the major optical losses, which are often in the form of light exiting the waveguide, and using Equation (S6) and (S7), Supporting Information, it can be seen that the optical loss in glass and PMMA is about 35% and 27%, respectively. Since the major contribution of optical losses is related to escape-cone losses,^[48] this difference in the amount and intensity of absorption and emission of light in two waveguides seems to come from this issue. This value is only related to the optical losses of escape cone in LSC. In general, self-absorption of light by the waveguide, light reflection from the waveguide, low light scattering in the waveguide, re-absorption of part of the light by the CQDs and also the difference in the hardness and structure of the waveguide surface can affect the optical losses.^[48–50]

Further spectral studies on the LSC made with CQDs at concentration of 3% CQDs showed that there is no significant difference in the absorption and emission spectra of CQDs after

mixing with PVP and depositing the layer on the waveguide (PMMA) (Figure 6). It indicates that the absorption and PL do not change by changing the concentration, and that the integration of CQDs in the LSC structure did not induce non-radiative recombination or quenching of CQDs. The small changes in the peak position of the absorption and emission spectra of CQDs in LSC compared to the absorption and emission spectra of CQDs in solution are most probably due to the change in the refractive index of the mixture containing CQDs/PVP after coating on the

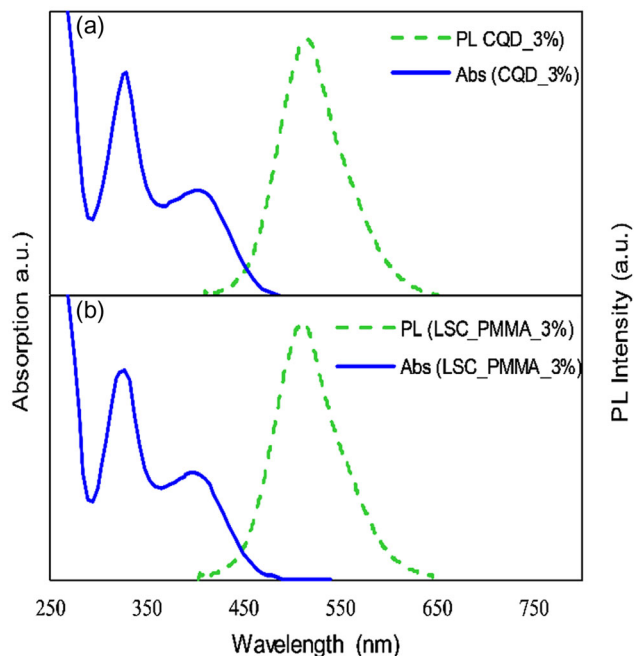


Figure 6. Normalized absorption and emission spectra of a) CQDs and b) LSC made with PMMA at a concentration of 3 wt% under 400 nm excitation wavelength.

waveguide.^[19] LSC emission was measured at different excitation wavelengths, which was similar to that of CQDs. The emission peak location remained unchanged, indicating that the emission properties CQDs remained constant after mixing with PVP (Figure 7a,b). Hence the structure and energy level of CQDs have not been affected by PVP polymer. Also, the measurement of the quantum yield of the CQDs/PVP mixture was unchanged at about 75%, showing the excellent stability of the synthesized CQDs in the polymer environment and the suitability of the integration procedure.

The dependence of PL emission at the edge of LSC on the distance from the excitation spot was measured in different optical paths to investigate the reabsorption losses. This work aims to investigate the effect of the distance traveled by the emitted light to the solar cell on optical losses. As shown in Figure 7b,c, the PL emission intensity of CQDs decreases with increasing distance from the edge, as expected, but the shape of the normalized PL spectra is not affected by the distance traveled by the light. This experimental evidence, with the absence of significant red shift, indicates very low reabsorption losses, guaranteed by the large Stokes shift (0.706 eV) of CQDs.^[51]

The photovoltaic and optical performance analysis of LSCs was performed according to the standards.^[52,53] The fabricated LSCs were measured under standard conditions (air mass AM 1.5G and ambient temperature 25 °C). The values η_{opt} and PCE of LSCs were calculated using Equation (S1), (S2), and (S3), Supporting Information.

The photovoltaic measurements show that increasing the number of layers from 1 to 4 the efficiency increases (Table 1 and Figure 7d,e). The increase in the optical efficiency, PCE, and current density can be clearly seen, which is due to the

increase in the optical absorption efficiency of the layer due to the increase in the thickness of the LSC. By increasing the number of layers to 5 layers a significant reduction in PCE and optical efficiency was observed, which seems to be caused by a decrease in the current density (Table 1 and Figure S8, Supporting Information). The decrease in current can be attributed to the deterioration of optical properties caused by the increase in optical density of the full LSC as its thickness increases. This result shows that the increase in efficiency due to the increase in the number of layers has a threshold.

From an engineering point of view, an alternative solution to the increase of the number of layers is the increase of the concentration of CQD in a single layer. Based on this, two concentrations of 3 and 5 wt% were chosen. Table 1 and the *I*-*V* curves of the fabricated LSCs (Figure S8, Supporting Information) show that, by increasing the concentration of CQDs from 1 to 3 wt%, a significant increase in PCE, optical efficiency, and current density is observed. LSC made with the concentration of 3 wt% in PMMA waveguide exhibit the following functional parameters: open circuit voltage of 0.52 V, current density of 4.66 mA cm⁻², optical efficiency of 6.5%, PCE of 1.6%, and geometric factor (*G*) of 2.08. In the glass waveguide, the functional parameters are as follows: open circuit voltage of 0.52 V, current density of 3.22 mA cm⁻², optical efficiency of 4.5%, PCE of 1.03%, and geometric factor, *G* of 2.08. By increasing the concentration of the CQDs to 5%, a sharp decrease in photovoltaic parameters is recorded. To elucidate this issue, the absorption and emission spectra of CQDs (Figure S6, Supporting Information) have to be considered. By increasing the CQD amount even through a single layer beyond threshold, there is a significant reduction in absorption and emission efficiency.

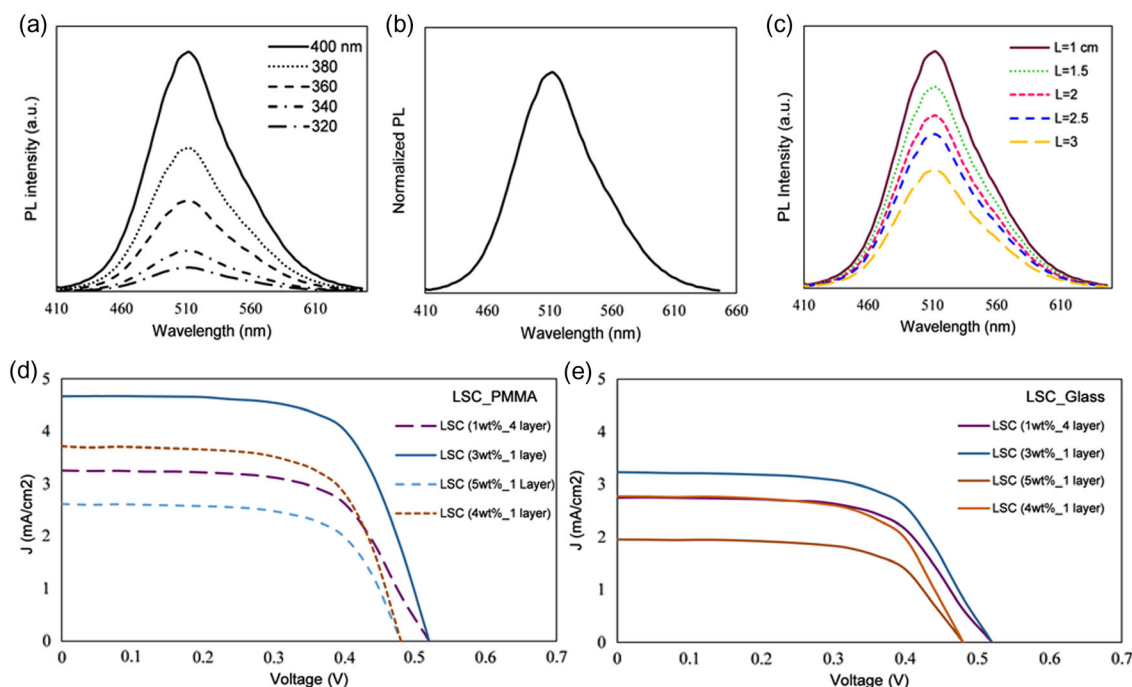


Figure 7. a) PL emission at different excitation wavelengths in LSC, indicating excitation wavelength-independent PL. b) Normalized PL spectra. c) PL spectra collected at the edge of LSC at different optical paths (*L* is the distance between the radiation location and the edge of the LSC in the direction of the optical fiber detector). d) Current–voltage curve of LSCs made with PMMA and e) glass in the highest performance samples.

Table 1. The parameters related to the photovoltaic characteristics of the fabricated LSCs and the silicon solar cell installed on the edges of the LSCs.

| Sample | Waveguide | V_{oc} [V] | J_{sc} [mA cm^{-2}] | FF [%] | η (% opt) | η (% overall) | G |
|---------------|-----------|--------------|----------------------------------|--------------|----------------|--------------------|-------------|
| 1 wt%_1 layer | PMMA | 0.52 | 3.06 | 63.02 | 4.27 | 1 | 2.08 |
| 1 wt%_2 layer | | 0.52 | 2.95 | 66.8 | 4.11 | 1.02 | 2.08 |
| 1 wt%_3 layer | | 0.52 | 3.15 | 65.7 | 4.4 | 1.07 | 2.08 |
| 1 wt%_4 layer | | 0.52 | 3.25 | 62.2 | 4.53 | 1.05 | 2.08 |
| 1 wt%_5 layer | | 0.52 | 3.07 | 62.64 | 4.3 | 1 | 2.08 |
| 3 wt%_1 layer | glass | 0.52 | 4.66 | 66.35 | 6.5 | 1.6 | 2.08 |
| 4 wt%_1 layer | | 0.48 | 3.71 | 65.58 | 5.47 | 1.23 | 2.08 |
| 5 wt%_1 layer | | 0.48 | 2.61 | 65.58 | 3.64 | 0.82 | 2.08 |
| Blank | | 0.48 | 1.09 | 60.26 | 1.53 | 0.31 | 2.08 |
| 1 wt%_1 layer | | 0.52 | 2.47 | 60.57 | 3.43 | 0.77 | 2.08 |
| 1 wt%_2 layer | | 0.52 | 2.46 | 60.9 | 3.43 | 0.78 | 2.08 |
| 1 wt%_3 layer | | 0.52 | 2.65 | 60.98 | 3.71 | 0.84 | 2.08 |
| 1 wt%_4 layer | | 0.52 | 2.74 | 61.45 | 3.83 | 0.87 | 2.08 |
| 1 wt%_5 layer | | 0.48 | 2.04 | 64.97 | 2.85 | 0.64 | 2.08 |
| 3 wt%_1 layer | | 0.52 | 3.23 | 61.56 | 4.5 | 1.03 | 2.08 |
| 4 wt%_1 layer | | 0.48 | 2.77 | 63.02 | 3.87 | 0.83 | 2.08 |
| 5 wt%_1 layer | | 0.48 | 1.95 | 63.02 | 2.72 | 0.59 | 2.08 |
| Blank | | 0.48 | 0.85 | 66.58 | 1.18 | 0.27 | 2.08 |
| Solar cell | | 0.58 | 34.39 | 61.08 | – | 12.18 | – |

In fact, by increasing the concentration from 1 to 5 wt%, we observe an initial increasing trend followed by a decrease in current density values, along with a decreasing trend in open circuit voltage. Regarding the voltage changes, it appears that with increasing concentration from 1 to 5 wt%, the voltage initially remains stable and then decreases. This slight voltage decrease is likely due to the increase in solar cell temperature at the edges, as voltage changes are typically more affected by temperature fluctuations in the cell.

The overall results show that the LSC fabricated with a concentration of 3 wt% has the highest current density, optical efficiency, and PCE among the other LSCs (Table 1 and Figure 7d,e).

The difference in photovoltaic and optical efficiency in two types of glass and PMMA waveguides is due to the difference in the amount of absorption and emission of CQDs. This difference is due to the difference in their refractive index, which determines the amplitude of the angle of the escape cone. Because an LSC has much larger dimension in real conditions, LSCs with dimensions of $15 \times 15 \times 0.6 \text{ cm}^3$ were fabricated on glass and PMMA substrates based on CQDs in the concentration of 3 wt%. For the fabrication of these large-area LSCs, we chose the optimal conditions obtained in the fabrication of small LSCs. The J - V curve of the fabricated LSCs, along with their images, are shown in Figure 8. As can be seen in Figure 8a, large-area LSC has very high transparency and strong emission in the visible region in the form of bright green (Figure 8b,c), which is consistent with the results of the previously discussed analyses.

The photovoltaic measurements showed that the LSC made with PMMA has an open circuit voltage of 0.52 V, the current

density of 3.245 mA cm^{-2} , the optical efficiency of 3.27%, and the PCE of 1.19% with a G of 6.25, which has the best values among large-area LSCs published up to now (Figure 8d and Table 2). It should be noted that the control or reference samples, referred to as BLANK, are LSCs fabricated without the incorporation of CQDs. This distinction is important for the comparative analysis of the performance and characteristics between the LSCs containing CQDs and the BLANK or control LSCs.

Examining the photovoltaic results obtained for LSCs made with glass and PMMA waveguides in two different geometric factors or different dimensions shows that by increasing the LSC area by nine times with the same thickness, the overall and optical efficiency decreased by 26% and 50% for PMMA, and 449% and 62% percent for glass, respectively. This is expected since the path for the emitted light to reach the edge of the LSC becomes much longer in large-area devices, which increases the possibility of light losses. In glass, larger losses are expected due to the lower refractive index. To show the effect of distance in LSCs with larger dimension, light emission was measured at the edges of LSC at different distances (Figure 8e). It can be seen that with increasing distance from the edge, no change in peak shift or shape of the normalized PL spectra was observed, which indicates the absence of energy loss due to light reabsorption and light reabsorption does not occur at different distances.^[51]

Comparison of the functional features obtained in this work with some of the most efficient LSCs based on CQDs is reported in Table 2, indicating the competitiveness of the device proposed in this research compared to the state of the art.

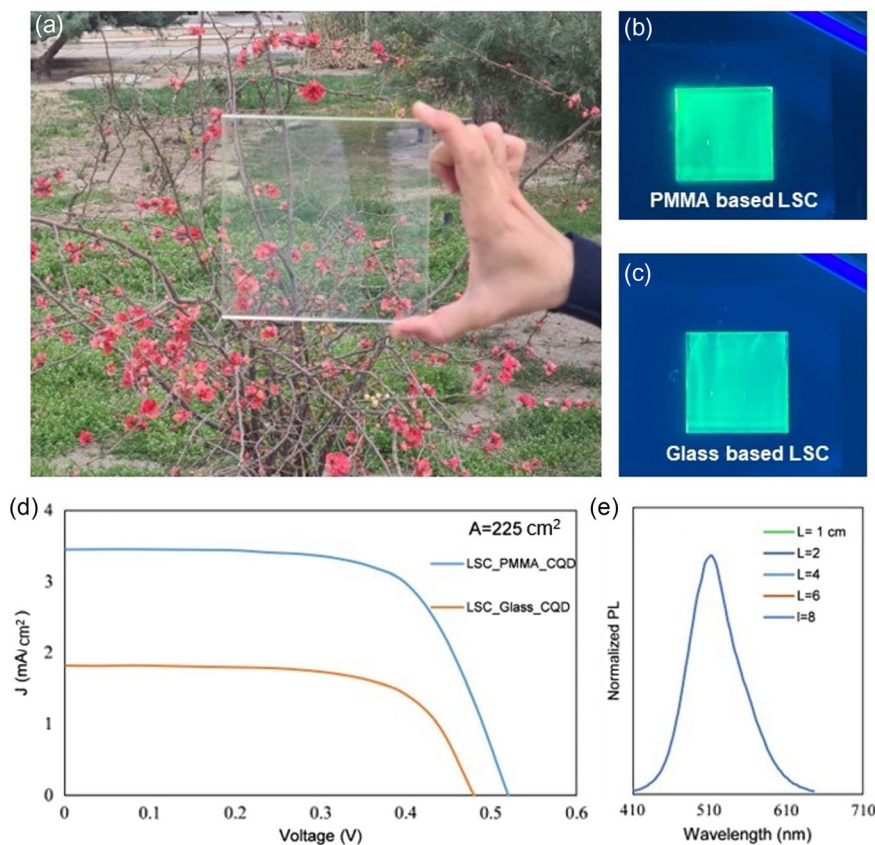


Figure 8. a) The high transparency of LSCs in the environment of Faculty of Agriculture in FUM university, and the light emission from the surface of LSCs can be clearly seen under UV light irradiation in b) PMMA and c) glass-based LSC. d) Current–voltage curve of $15 \times 15 \times 0.6 \text{ cm}^3$ with glass and PMMA waveguides. e) Normalized PL of different optical distances in the direction of the optical fiber detector.

Table 2. Comparison of the optical efficiency of LSCs of this research with some of the most important works done in the field of LSCs based on CQDs.

| References | η_{Opt} [%] | LSC area [cm^2] | G factor | LSC |
|------------|-------------------------|----------------------------|----------------|---|
| This work | 6.5 | 25 | 6.25 | Optimized LSC based on CQD (waveguide: PMMA) |
| This work | 3.27 | 225 | 2.83 | Optimized LSC based on CQD (waveguide: PMMA) |
| This work | 4.5 | 25 | 6.25 | Optimized LSC based on CQD (waveguide: glass) |
| This work | 1.73 | 225 | 2.83 | Optimized LSC based on CQD (waveguide: glass) |
| [19] | 2.2 | 225 | 2.5 | LSC-based vacuum heating CQD |
| [54] | 4.65 | 100 | ≈ 2.66 | LSC-based CQD |
| [21] | 2.3 | 64 | – | CQD-based tandem LSC |
| [24] | 4.8 | 25 | 6.25 | LSC-based silicon doped CQD |
| [55] | 3.76 | 6.25 | 3.12 | Carbon dots and perovskite quantum dots |
| [56] | 4.8 | 100 | 4.8 | LSC-based red emissive CQD |

3.4. Investigating the Stability of the Fabricated LSCs

The stability of LSCs was tested for 90 days from June 22, 2022, until September 22, 2022, in Tehran. They were exposed to air and under light in the outdoor environment (Figure S5, Supporting Information, see experimental section in Supporting Information). Every 15 days PCE and optical

efficiency were measured (Figure 9a,b). Measurements related to PCE and optical efficiency of LSCs show that there is no significant difference in overall efficiency and optical efficiency. This important evidence is due to the extraordinary stability of the synthesized CQDs, which does not suffer from the drop in optical performance in real conditions, and shows the importance of using CQDs and their high capability in LSCs.

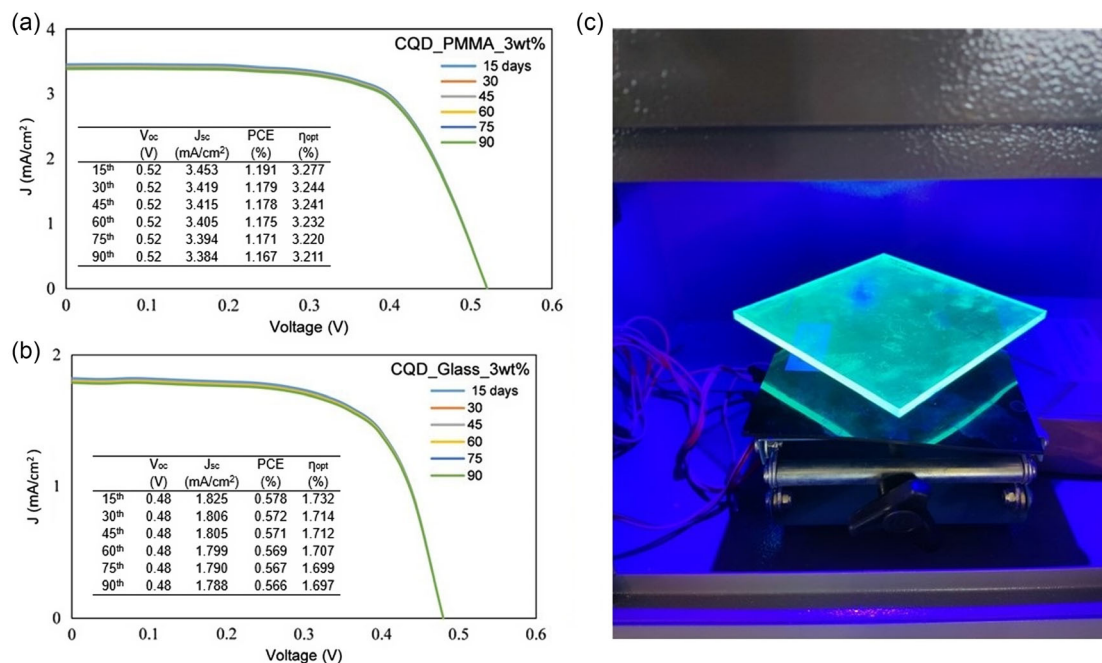


Figure 9. Current–voltage curve of LSCs made with a) PMMA and b) glass ($15 \times 15 \times 6 \text{ cm}^3$) during 90 days. c) Image of LSC made with CQDs with PMMA after 90 days under UV light.

The image of the edge emission of the fabricated concentrators after 90 days is shown in Figure 9c, which shows the bright emission intensity. Photovoltaic studies showed that after 90 days, the photovoltaic and optical efficiency in the LSCs made has dropped by almost 2%. It should be noted that the stability of LSCs was investigated without any protection or special coating.

3.5. Investigating the Temperature Characteristics of the Greenhouse Built with LSC Roof

Small prototype greenhouses with dimensions of $15 \times 15 \times 15 \text{ cm}^3$ were built and tested. These greenhouses are in four models, including a greenhouse with a normal glass roof, with a normal PMMA roof, with an LSC roof based on CQDs with glass waveguides, and with an LSC roof based on CQDs with PMMA waveguides (see experimental section in Supporting Information). The greenhouses were placed under the solar simulator (Figure S4b, Supporting Information). The issue of temperature and its control in different seasons of the year is one of the most important and vital parameters in the greenhouse. The purpose of this part is to investigate the effect of greenhouse covers based on LSC technology made with CQDs. The temperature inside the greenhouse was recorded by a thermometer every 4 min under solar simulator (AM 1.5G). After 60 min, the greenhouse was removed under the solar simulator and its internal temperature was recorded every 4 min for 60 min. The greenhouse was located in a laboratory environment. In this part, the process of temperature increase inside the greenhouse environment under the solar simulator and the temperature decrease inside the greenhouse after irradiation were investigated. As shown in Figure 10a,b the comparison of

the obtained experimental results shows that a significant temperature difference was recorded. The greenhouse with LSC roof based on CQDs made with PMMA waveguide has faced a lower temperature increase (from 25.2 to 41.6 °C) compared to greenhouses made with LSC based on glass (25.3–45.13 °C) and normal roofs made with glass (25.6–44.6 °C) and normal PMMA (24.4–44.9 °C). In the best case, in the greenhouse with an LSC roof based on CQDs with PMMA waveguide, compared to the greenhouse with normal PMMA roof, the air temperature inside the greenhouse is 3.3 °C cooler after 1 h of simulated sunlight irradiation. This important result shows that it is possible to use photovoltaic covers with PMMA waveguide or glass waveguide according to the weather conditions of a region. For example, in areas where the radiation intensity is high and it is necessary to make the greenhouse environment cooler for growing plants, LSC based on CQDs with PMMA waveguides can be useful in the construction of photovoltaic greenhouses, and in areas with low radiation intensity that it is necessary to make the greenhouse environment warmer, LSC based on CQDs with glass waveguide is more useful. With this approach, in addition to providing a part of the energy needs of the greenhouse itself, it is possible to make the space inside the greenhouse significantly cooler or warmer according to the weather conditions of the region. Although this temperature difference is about a few degrees, it was recorded in a space with dimensions of $3 \times 10^{-3} \text{ m}^3$, which will definitely have greater effects in larger spaces. It is probably related to the absorption and emission intensity of glass and PMMA in the presence of CQDs. In the absorption and emission intensity curves the absorption in glass with a layer containing CQDs is far less than PMMA with a layer containing CQDs. Therefore, more light passes through the

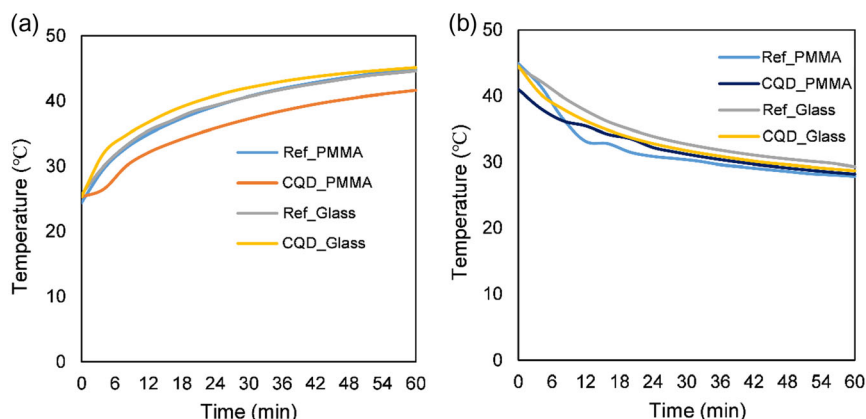


Figure 10. a) Increase and b) decrease of internal temperature of the greenhouse during simulated solar light irradiation (AM 1.5G). The greenhouses were under the solar simulator for 60 min, and after they were removed from the solar simulator, the internal temperature was recorded every 4 min.

surface of the glass and enters the greenhouse, while in the greenhouse with a roof made of PMMA with CQDs layer, more light is absorbed and participates in the process of light emission and power generation. This problem can be one of the important reasons for the hotter greenhouse with a roof made with LSC based on glass waveguide containing CQDs. Also, the greenhouse with a glass roof containing CQDs, due to the lower refractive index in comparison with PMMA, instead of emitting all the light to the edges of the waveguide, a part of the emitted light, which is actually the light with a longer and warmer wavelength, is released on the surface of the glass. This light emitted on the surface enters the greenhouse and is effective in warming the environment. Based on this, the greenhouse built with LSC roof based on PMMA containing CQDs, due to the lower loss rate, absorbs more of the light instead of passing through it, and with the light emission and arrival of the emitted light to the edges of the waveguide and solar cell, it causes power generation. In fact, in this greenhouse, the light is used more to produce power than to heat the greenhouse, that is why the internal temperature of the greenhouse is cooler. The incorporation of CQDs into the greenhouse roof structure enables the selective conversion and guidance of incident solar radiation, improving temperature regulation within the greenhouse environment. The CQDs absorb a portion of the non-useful, higher-energy UV light and re-emit it as longer-wavelength, more useful visible light. The choice of waveguide material, such as PMMA, with a suitable refractive index, facilitates the efficient guidance of this re-emitted light toward the edges of the structure. Here, the light can be effectively captured and converted into electrical energy by integrated solar cells, rather than being released back into the greenhouse interior and contributing to heating. In contrast to a control greenhouse without CQDs, where most incident solar radiation directly enters the greenhouse, the CQD-integrated system selectively filters and redirects a portion of the light toward electricity generation. This results in a lower internal temperature within the greenhouse, as less of the absorbed solar energy is directly converted into heat. The synergistic effects of the CQD optical properties, the waveguide material characteristics, and the integration of the LSC structure with edge-mounted solar cells are key factors enabling this temperature regulation capability.

The results of this section show that the use of LSCs in the construction of transparent photovoltaic covers for greenhouses, while meeting the plant's light needs and generating electricity, can have a significant effect on the internal temperature of greenhouse.

The implementation of this technology in the development of transparent photovoltaic covers for large-scale commercial greenhouses holds significant potential. Such an application could effectively improve the temperature conditions within the greenhouse environment by regulating heat and light transmission. This, in turn, creates a more stable and conducive environment for plant growth, enhancing crop yields and quality. Also, integrating photovoltaic covers can contribute to meeting a portion of the greenhouse's energy consumption requirements. By harnessing solar energy, these covers can generate electricity to power various greenhouse operations, such as lighting, heating, ventilation, and irrigation systems. This dual benefit not only enhances product growth but also significantly reduces the overall energy demands of the greenhouse operation, resulting in a more sustainable and efficient system. Moreover, the reduction in external energy dependency and operational costs aligns with the increasing focus on sustainable agricultural practices. It also offers economic advantages by lowering energy bills and potentially providing surplus energy back to the grid. The ability to combine agricultural productivity with renewable energy generation positions this technology as a transformative solution for modern agriculture, contributing to food security and environmental conservation.

4. Conclusion

We developed transparent photovoltaic covers for greenhouses using the LSC technology based on CQDs. CQDs were synthesized using a fast, cheap, and scalable method with a high quantum yield (75%) and large Stokes shift (0.706 eV). Additionally, a comprehensive study of LSCs engineering was conducted, focusing on the most crucial parameters in LSC fabrication, such as waveguide type, lumino-phore concentration, and the number of luminescent layers. The LSCs were fabricated in two sizes of

$5 \times 5 \times 0.6$ and $15 \times 15 \times 0.6 \text{ cm}^3$. Photovoltaic and optical investigations revealed that increasing the luminophore concentration in one layer gives much better results than increasing the number of layers for a fixed concentration. Finally, the best LSCs result in optical efficiency of 6.5% and PCE of 1.6%, with a geometric factor of 2.08. The optimized large-area ($15 \times 15 \times 0.6 \text{ cm}^3$) LSC fabrication results in optical efficiency and PCE as high as 3.27% and 1.19%, respectively. The use of scalable method for the synthesis of CQDs with a high quantum yield and optimized LSC fabrication led to a higher optical yield and overall efficiency, compared to previous works. Long lifetime and excellent optical and environmental stability after 90 days indicate the superior capability of CQDs for LSC fabrication. In addition, the thermal characterization of a small-scale greenhouse with an LSC roof showed the efficacy of LSC to control the temperature inside the greenhouse. Our comprehensive methodology can provide a very good balance between energy production and supplying the light needs of the plant in the greenhouse. This can potentially result in sustainable food production in modern greenhouses integrated with LSC and Photovoltaic technologies, and make it a viable commercial option.

Supporting Information

Supporting Information is available from the Wiley Online Library or from the author.

Acknowledgements

This work was supported by the Ferdowsi University of Mashhad and Iran National Science Foundation (INFS) (No. 99012691). A.V. acknowledges the Knut & Alice Wallenberg Foundation, the LTU Lab fund program, the Kempe Foundation and the Italian Ministry of University and Research for partial funding through PNRR NEST project.

Conflict of Interest

The authors declare no conflict of interest.

Author Contributions

Kambiz Hosseinpahani: Conceptualization (equal); Data curation (lead); Formal analysis (lead); Investigation (equal); Methodology (lead); Writing—original draft (lead). **Mohammad Hossein Abbaspour-Fard:** Conceptualization (supporting); Resources (equal); Writing—review & editing (equal). **Mahmoud Reza Golzarian:** Formal analysis (lead); Writing—review & editing (equal). **Elaheh K. Goharshadi:** Formal analysis (equal); Supervision (supporting); Writing—original draft (supporting). **Alberto Vomiero:** Conceptualization (equal); Funding acquisition (equal); Writing—review & editing (lead).

Data Availability Statement

The data that support the findings of this study are available from the corresponding author upon reasonable request.

Keywords

agrivoltaic, carbon quantum dots, luminescent solar concentrator, photovoltaic greenhouses

Received: June 14, 2024

Revised: July 23, 2024

Published online:

- [1] G. Lages Barbosa, F. D. Almeida Gadelha, N. Kublik, A. Proctor, L. Reichelm, E. Weissinger, G. M. Wohlleb, R. U. Halden, *Int. J. Environ. Res. Public Health* **2015**, *12*, 6879.
- [2] C. S. Allardyce, C. Fankhauser, S. M. Zakeeruddin, M. Grätzel, P. J. Dyson, *Sol. Energy* **2017**, *155*, 517.
- [3] Z. Li, A. Yano, H. Yoshioka, *Appl. Energy* **2020**, *279*, 115853.
- [4] Z. Li, A. Yano, M. Cossu, H. Yoshioka, I. Kita, Y. Ibaraki, *J. Agric. Meteorol.* **2018**, *74*, 114.
- [5] R. H. E. Hassanien, M. M. Ibrahim, A. E. Ghaly, E. N. Abdelrahman, *Heliyon* **2022**, *8*, e08877.
- [6] M. Cossu, L. Ledda, P. A. Deligios, A. Sirigu, L. Murgia, A. Pazzona, A. Yano, *Acta Horticulturae*, International Society for Horticultural Science (ISHS), Leuven, Belgium **2017**, pp. 47–56.
- [7] S. Moretti, A. Marucci, *Energies* **2019**, *12*, 2589.
- [8] F. Blando, C. Gerardi, M. Renna, S. Castellano, F. Serio, *J. Berry Res.* **2018**, *8*, 55.
- [9] M. Kadowaki, A. Yano, F. Ishizu, T. Tanaka, S. Noda, *Biosyst. Eng.* **2012**, *111*, 290.
- [10] L. Lu, M. Effendy Ya'acob, M. Shamsul Anuar, M. Nazim Mohtar, *Sustainable Energy Technol. Assess* **2022**, *52*, 102077.
- [11] R. B. Alnoman, E. Nabil, S. Parveen, M. Hagar, M. Zakaria, *RSC Adv.* **2022**, *12*, 11420.
- [12] D. Benetti, F. Rosei, *Nanoenergy Adv.* **2022**, *2*, 222.
- [13] C. Corrado, S. W. Leow, M. Osborn, I. Carbone, K. Hellier, M. Short, G. Alers, S. A. Carter, *J. Renewable Sustainable Energy* **2016**, *8*, 43502.
- [14] O. Essahili, M. Ouafi, O. Moudam, *Sol. Energy* **2022**, *245*, 58.
- [15] N. Roslan, M. E. Ya'acob, M. A. M. Radzi, Y. Hashimoto, D. Jamaludin, G. Chen, *J. Renewable Sustainable Energy* **2018**, *92*, 171.
- [16] D. Ursu, M. Vajda, M. Miclau, *Int. J. Energy Res.* **2022**, *46*, 18550.
- [17] J. Keil, Y. Liu, U. Kortshagen, V. E. Ferry, *ACS Appl. Energy Mater.* **2021**, *4*, 14102.
- [18] L. Shen, R. Lou, Y. Park, Y. Guo, E. J. Stallknecht, Y. Xiao, D. Rieder, R. Yang, E. S. Runkle, X. Yin, *Nat. Food* **2021**, *2*, 434.
- [19] H. Zhao, G. Liu, S. You, F. V. A. Camargo, M. Zavelani-Rossi, X. Wang, C. Sun, B. Liu, Y. Zhang, G. Han, *Energy Environ. Sci.* **2021**, *14*, 396.
- [20] R. Mazzaro, A. Vomiero, *Adv. Energy Mater.* **2018**, *8*, 1801903.
- [21] L. Zdražil, S. Kalytchuk, K. Holá, M. Petr, O. Zmeškal, Š. Kment, A. L. Rogach, R. Zbořil, *Nanoscale* **2020**, *12*, 6664.
- [22] Y. Zhou, D. Benetti, X. Tong, L. Jin, Z. M. Wang, D. Ma, H. Zhao, F. Rosei, *Nano Energy* **2018**, *44*, 378.
- [23] L. Gao, C. Wang, S. Xu, P. Xia, F. Liu, H. Sun, Z. Wang, C. Lu, Y. Cui, *ACS Appl. Nano Mater* **2022**, *5*, 7850.
- [24] X. Gong, S. Zheng, X. Zhao, A. Vomiero, *Nano Energy* **2022**, *101*, 107617.
- [25] F. Mateen, M. Ali, H. Oh, S.-K. Hong, *Sol. Energy* **2019**, *178*, 48.
- [26] J. Wu, W. Xin, Y. Wu, Y. Zhan, J. Li, J. Wang, S. Huang, X. Wang, *Chem. Eng. J.* **2021**, *422*, 130158.
- [27] M. Shimoda, K. Honda, *Appl. Entomol. Zool.* **2013**, *48*, 413.
- [28] M. Raviv, Y. Antignus, *Photochem. Photobiol.* **2004**, *79*, 219.
- [29] K. Zuk-Golaszewska, M. K. Upadhyaya, J. Golaszewski, *Plant Soil Environ.* **2003**, *49*, 135.

- [30] D. Zhou, P. Jing, Y. Wang, Y. Zhai, D. Li, Y. Xiong, A. V. Baranov, S. Qu, A. L. Rogach, *Nanoscale Horiz.* **2019**, *4*, 388.
- [31] J. Wei, Q. Lou, J. Zang, Z. Liu, Y. Ye, C. Shen, W. Zhao, L. Dong, C. Shan, *Adv. Opt. Mater.* **2020**, *8*, 1901938.
- [32] Y. Zheng, J. Zheng, J. Wang, Y. Yang, T. Lu, X. Liu, *Nanomaterials* **2020**, *10*, 303.
- [33] Y. Chen, M. Zheng, Y. Xiao, H. Dong, H. Zhang, J. Zhuang, H. Hu, B. Lei, Y. Liu, *Adv. Mater.* **2016**, *28*, 312.
- [34] Y. Ru, G. I. N. Waterhouse, S. Lu, *Aggregate* **2022**, *3*, e296.
- [35] M. Park, Y. Jeong, H. S. Kim, W. Lee, S. Nam, S. Lee, H. Yoon, J. Kim, S. Yoo, S. Jeon, *Adv. Funct. Mater.* **2021**, *31*, 2102741.
- [36] K. Hola, M. Sudolská, S. Kalytchuk, D. Nachtigallová, A. L. Rogach, M. Otyepka, R. Zboril, *ACS Nano* **2017**, *11*, 12402.
- [37] S. Lu, L. Sui, J. Liu, S. Zhu, A. Chen, M. Jin, B. Yang, *Adv. Mater.* **2017**, *29*, 1603443.
- [38] Z. Xing, Z. Ju, Y. Zhao, J. Wan, Y. Zhu, Y. Qiang, Y. Qian, *Sci. Rep.* **2016**, *6*, 26146.
- [39] P. Huang, S. Xu, M. Zhang, W. Zhong, Z. Xiao, Y. Luo, *Phys. Chem. Chem. Phys.* **2019**, *21*, 26133.
- [40] S. Lu, G. Xiao, L. Sui, T. Feng, X. Yong, S. Zhu, B. Li, Z. Liu, B. Zou, M. Jin, *Angew. Chem.* **2017**, *129*, 6283.
- [41] S. Qu, X. Liu, X. Guo, M. Chu, L. Zhang, D. Shen, *Adv. Funct. Mater.* **2014**, *24*, 2689.
- [42] H. J. Yoo, B. E. Kwak, D. H. Kim, *J. Phys. Chem. C* **2019**, *123*, 27124.
- [43] X. Zhang, Y. Liu, C.-H. Kuan, L. Tang, T. D. Krueger, S. Yeasmin, A. Ullah, C. Fang, L.-J. Cheng, *J. Mater. Chem. C* **2023**, *11*, 11476.
- [44] Y. Choi, B. Kang, J. Lee, S. Kim, G. T. Kim, H. Kang, B. R. Lee, H. Kim, S.-H. Shim, G. Lee, *Chem. Mater.* **2016**, *28*, 6840.
- [45] S. Qu, D. Zhou, D. Li, W. Ji, P. Jing, D. Han, L. Liu, H. Zeng, D. Shen, *Adv. Mater.* **2016**, *28*, 3516.
- [46] J. Wang, Y. Yang, X. Liu, *Mater. Adv.* **2020**, *1*, 3122.
- [47] Y. Zhang, P. Zhuo, H. Yin, Y. Fan, J. Zhang, X. Liu, Z. Chen, *ACS Appl. Mater. Interfaces* **2019**, *11*, 24395.
- [48] M. G. Debije, P. P. C. Verbunt, B. C. Rowan, B. S. Richards, T. L. Hoeks, *Appl. Opt.* **2008**, *47*, 6763.
- [49] S. McDowall, T. Butler, E. Bain, K. Scharnhorst, D. Patrick, *Appl. Opt.* **2013**, *52*, 1230.
- [50] L. R. Wilson, *Ph.D. Thesis, Heriot-watt University* **2010**.
- [51] Z. Wang, X. Zhao, Z. Guo, P. Miao, X. Gong, *Org. Electron.* **2018**, *62*, 284.
- [52] M. G. Debije, R. C. Evans, G. Griffini, *Energy Environ. Sci.* **2021**, *14*, 293.
- [53] C. Yang, D. Liu, R. R. Lunt, *Joule* **2019**, *3*, 2871.
- [54] J. Li, H. Zhao, X. Zhao, X. Gong, *Nanoscale Horiz.* **2023**, *8*, 83.
- [55] C. Cai, M. Wang, J. Wang, B. Xu, J. Wang, L. Zhang, W. Xin, L. Xue, J. Li, X. Wang, *Appl. Surf. Sci.* **2023**, *609*, 155313.
- [56] G. Liu, M. Zavelani-Rossi, G. Han, H. Zhao, A. Vomiero, *J. Mater. Chem. A* **2023**, *11*, 8950.